

Inorganic Pyrophosphate at Serum Concentration May Not Be Able to Inhibit Mineralization: A Study in Aqueous Solutions and Serum

Yuxuan Cheng, Jing Ru, Chaobo Feng, Xiaohao Liu, Hua Zeng, Shuo Tan, Xi Chen,* Feng Chen,* and Bing-Qiang Lu*



Cite This: *ACS Omega* 2024, 9, 17334–17343



Read Online

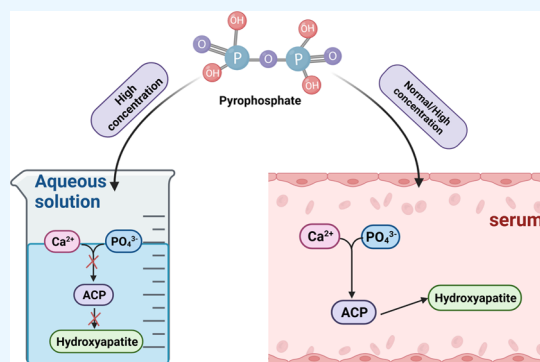
ACCESS |

Metrics & More

Article Recommendations

Supporting Information

ABSTRACT: The constituent ions of calcium phosphate in body fluids are in the supersaturated state and tend to form minerals physiologically or pathologically. Inorganic pyrophosphate (PPi) has been considered as one of the most important inhibitors against the formation of calcium phosphate minerals. However, serum PPi concentrations in humans are maintained at a level of several $\mu\text{mol/L}$, and its effectiveness and mechanism for mineralization inhibition remain ambiguous. Therefore, this work studied the mineralization process in an aqueous solution, explored the effective inhibitory concentration of PPi by titration, and characterized the species during the reactions. We find that PPi at a normal serum concentration does not inhibit mineralization significantly. Such a conclusion was further confirmed in the PPi-added serum. This work indicates that PPi may not be a major direct inhibitor of mineralization in serum and possibly functions via alternative mechanisms.



1. INTRODUCTION

Biomineralization is an essential physiological process in human body that produces biominerals (mainly calcium phosphate) in specific tissues and is a key step toward the formation of hard tissue.¹ From a chemical perspective, bone tissue is composed of organic and inorganic substances, and the main component of inorganic substances is hydroxyapatite (HAP, a form of calcium phosphate), which are responsible for certain biological and mechanical functions of the body.^{2–4} It is generally accepted that biomineralization proceeds through a series of intermediates, ranging from prenucleation species^{5,6} and amorphous solids^{7–9} to nano/microcrystals,^{10,11} which then progress to stable forms.¹² Proteins (e.g., OPN,¹³ matrix GLA) and cells (e.g., osteoblasts, ameloblast, chondrocytes,¹⁴ smooth muscle cells,¹⁵ endothelial cells^{16,17}) are involved in regulating the mineralization process.¹⁴ In addition to normal physiological mineralization, ectopic mineralization also occurs in human body, generating calcium salt deposits at tendon attachments,¹⁸ vessel walls,^{19,20} skin,²¹ brain parenchyma,²² etc., and often leading to clinical symptoms.

The constituent ions of biominerals in the body fluids are in a supersaturate and dynamic state.²³ Serum phosphate concentrations usually fluctuate in the range of 1.0–1.4 mmol/L,^{24–26} and serum calcium is in 2.3–2.8 mmol/L.^{27,28} In contrast, when the concentrations of PO_4^{3-} or Ca^{2+} are abnormally elevated, such as in patients with hyperphosphatemia where serum inorganic phosphate can be 5.0 mmol/L, the body is susceptible to high mineralization pressure and

thus more susceptible to ectopic mineralization.^{29,30} In this case, as one of the adverse consequences, the so-called calprotectin tends to form via the mineralization of specific proteins in the serum (e.g., fetuin-A),³¹ which would eventually cause abnormal calcification of blood vessels, kidneys, etc.,³² if the excretion function of calprotectin is disturbed. In serum,³³ various mineralization inhibitors, such as ATP,³⁴ fetuin-A,³⁵ vitamin K,³⁶ matrix GLA,³⁷ and pyrophosphates (PPi),³⁸ are required to resist the mineralization pressure derived from the supersaturated mineral ions. Among them, PPi is believed to be very essential, especially in resistance against ectopic mineralization. Each PPi molecule consists of two inorganic phosphates (Pi) linked by a hydrolyzable ester bond and is a byproduct of a variety of biochemical reactions.³⁹ It is mainly produced by the hydrolysis of phosphodiester bonds in nucleotide triphosphates (e.g., adenosine triphosphate (ATP) or uridine triphosphate (UTP))³⁸ and widely distributed in the whole body. In serum, PPi is at the concentrations of about 0.58–3.78 $\mu\text{mol/L}$.^{40,41} Generally, over 60% of the plasma PPi is derived from nucleoside triphosphates (NTPs) extruded by the ABC

Received: December 27, 2023

Revised: March 20, 2024

Accepted: March 28, 2024

Published: April 6, 2024



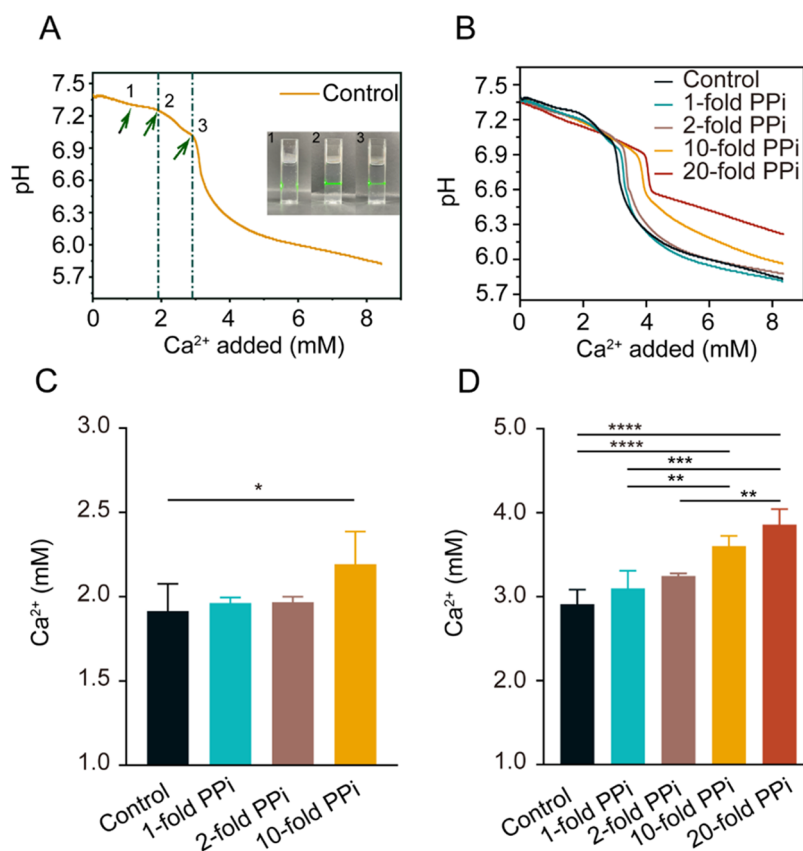


Figure 1. (A) pH change during the titrations in a 2.00 mM Pi solution without PPI (control). The inflections between the change steps of the pH curves are confirmed with the aid of differential processing. Inset: Tyndall effect tests of the titration solutions at different time points labeled with numbers (1, 2, 3) on the pH curve: before the first pH inflection (1), the first pH inflection (2), and the second pH inflection (3). (B) pH changes during the titrations in the Pi solutions containing different amounts of PPI. (C, D) Statistical concentrations of added Ca²⁺ required to reach the first (C) and second (D) pH inflection points. **p* < 0.05, ***p* < 0.01, ****p* < 0.001, *****p* < 0.0001, and *p* ≥ 0.05 are not labeled with asterisks.

transporter protein ABCC6.^{42–44} ENPP also acts in maintaining plasma PPI concentrations by breaking down ATP into adenosine monophosphate (AMP) and PPI. The abnormalities in PPI-related biological molecules are associated with severe ectopic mineralization in vivo. For example, generalized arterial calcification of infancy (GACI) can be caused by a mutation of NPP1, which results in reduced enzyme activity of NPP1, decreased PPI production, and accumulation of mineralized and fragmented elastic fibers of the connective tissue in the skin.^{45,46} Besides, inactivating mutations in ABCC6 usually result in pseudoxanthoma elasticum (PXE),⁴⁷ an autosomal recessive disease in which circulating PPI is significantly reduced, leading to progressive ectopic mineralization of the matrix in the skin, eyes, and arteries.^{45,46}

However, it remains unclear how PPI plays a role in suppressing mineralization in serum. Considering that the serum concentration of PPI is as low as several μM, nearly 1000-fold lower than that of Pi as introduced above, it raises the question whether such trace amounts of PPI are effective in mineralization inhibition, especially when calcium and phosphorus concentrations in the physiological environment are abnormally elevated. Herein, from the perspective of the chemical reaction (Ca²⁺ and Pi react to form calcium phosphate), we investigated the effect of PPI on mineralization inhibition in the aqueous ion solutions and real serum. Specifically, titration was applied to study the reaction process of calcium and Pi ions in solutions, where PPI with a concentration identical to or higher than that in serum was

included to study its influence on the mineral formation. Then, in real serum, the effect of PPI on mineralization inhibition was further investigated. We find that in the solutions containing both normal and higher concentrated Pi, the PPI at serum concentration does not inhibit mineralization effectively, suggesting that PPI may not be the primary direct inhibitor of mineralization in serum, or it functions via alternative mechanisms.

2. RESULTS AND DISCUSSION

2.1. Ability of PPI to Inhibit Mineralization in Solutions Containing Normal Pi Concentration. Titration is a common strategy used for studying the formation processes of biominerals, (e.g., calcium phosphate,^{48,49} calcium carbonate,^{48,50} iron oxide,⁵¹ etc.). By measuring ion concentrations, pH changes, turbidity, etc. during titration, it is possible to track the reaction kinetics, capture the formed species, and ultimately uncover the underlying mineralization mechanisms. Mineralization in human body fluids predominantly involves the chemical reaction between Ca²⁺ and Pi, by which calcium phosphate minerals are formed in different tissues. Here, the mineralization process by the chemical reaction between Ca²⁺ and Pi was investigated via a titration, where the Ca²⁺ solution was slowly dropped in the Pi solution to initiate the reaction; meanwhile, a variety of analyses were conducted. The total Pi concentration in human serum is ~3.9 mmol/L, of which only 0.8–1.3 mmol/L is in the inorganic form and the rest is in the organic compounds including

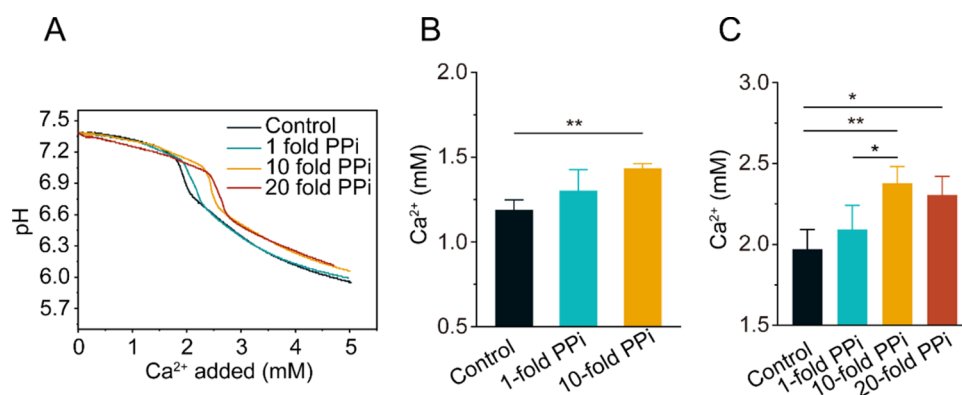


Figure 2. (A) pH changes during the titrations in 5.00 mM Pi solutions containing different amounts of PPI. (B, C) Statistical concentrations of added Ca²⁺ required to reach the first (B) and second (C) pH inflection points. * $p < 0.05$, ** $p < 0.01$, and $p \geq 0.05$ are not labeled with asterisks.

phospholipids.²⁴ Considering the dilution caused by adding Ca²⁺ solution into Pi solution during the titration, we chose a slightly higher concentration than that in the body fluid, i.e., 2.00 mM Pi (from Na₂HPO₄) solution, to simulate the serum Pi.

We find that titration in the way of pH-constant/monitoring Ca²⁺ activity is difficult to achieve, as we fail to precisely control the pH at the neutral value (7.40) during titration in such a solution, probably due to the weak buffer effect of the low Pi concentration (usually, it is higher than 10 mM in the previous studies^{52,53}). Fortunately, the pH change (without fixing the pH) during titration can also accurately reflect the occurrences of nucleation and crystallization. As shown in Figure 1A, when continuously adding Ca²⁺ solution (0.05 M) into Pi solution (2.00 mM), the pH value drops in steps accordingly (the turning points denoted as inflections were confirmed by differential processing of the pH curves). In the first step, from pH 7.40 to 7.24, the solution appears transparent and has no visible Tyndall scattering, indicating a prenucleation period of this step. When the concentration of added Ca²⁺ reaches 1.92 mM (pH = 7.25), an inflection on the smooth pH curve appears, where we observe significant turbidity and Tyndall scattering (Figure 1A). This reveals that the nucleation occurs at the inflection and the CaP minerals begin to form. At 2.93 mM added Ca²⁺ (pH = 7.00), the slowly decreasing curve becomes steep, and the second inflection is observed where the pH changes more abruptly than in the first one, which should corresponds to the crystallization as we discuss below (Figure 1). Therefore, the nucleation and crystallization can be represented with the first and second inflections on the pH curves, respectively.

Based on the experiments above (set as the control), we further introduced PPI at different concentrations into the Pi solution and then investigated their influences on the formation process of calcium phosphate minerals during titration. In the presence of PPI (concentrations are expressed as 1-fold, 2-fold, 10-fold, and 20-fold, standing for 1, 2, 10, and 20 times that in human serum, namely 1.7, 3.4, 17, and 34 μ M PPI, respectively), we find that the profiles of the pH change are similar to that without PPI (Figure 1B), but the nucleation and crystallization are delayed (Figure 1C vs D). Again, the nucleation and crystallization can be confirmed by the observation of the turbidity and Tyndall scattering of the solution as well as the characterization in the following, that is, before the first pH inflection, the solution is transparent, but after that, it becomes turbid.

By repeating the titration at least three times at each PPI concentration, we obtain the statistical added Ca²⁺ concentrations at the events of nucleation and crystallization, which also reflect the relative time differences for such events since Ca²⁺ is added at a constant rate during the titrations. In the solution containing 1-fold and 2-fold PPI, the nucleation is not delayed significantly compared to that of the control (without PPI). Specifically, the 1-fold PPI group shows the first pH inflection at a Ca²⁺ concentration of 1.96 ± 0.03 mM, which is not statistically different ($p > 0.05$) from the control (1.92 ± 0.16 mM). However, the addition of 10-fold PPI leads to a delay in nucleation ($p < 0.05$), with the first pH inflection occurring at 2.19 ± 0.19 mM Ca²⁺ (Figure 1C). Further increasing the PPI concentration to 20-fold, we cannot observe the first pH inflection, but the solution becomes turbid at the point similar to that of 10-fold.

PPI also has a delay effect on crystallization in the solutions. As shown in Figure 1D, the 1-fold PPI group requires 3.10 ± 0.21 mM Ca²⁺ to reach the second inflection point (crystallization) of the pH curve, which is about 0.19 mM higher than that required in the control group (2.91 ± 0.17 mM) ($p > 0.05$). The 2-fold PPI group exhibits similarity to that of 1-fold ($p > 0.05$). Upon adding 10-fold PPI, 3.60 ± 0.12 mM Ca²⁺ is required to reach the second pH inflection, which is 0.69 mM higher than that of the control group ($p < 0.0001$). The addition of 20-fold PPI is more pronounced ($p < 0.0001$), requiring 3.86 ± 0.19 mM Ca²⁺ to reach the second inflection of pH, which is 0.95 mM Ca²⁺ higher than that of the control group (Figure 1D).

While it is reported that PPI is a critical inhibitor against mineralization,³⁸ we find that PPI at normal serum concentration (1.7 μ M) is not as effective as expected in these investigated Pi solutions. Only after increasing its concentration to a much higher level, e.g., 10-fold, there is a significant delay of nucleation and crystallization observed.

2.2. Ability of PPI to Inhibit Mineralization in Solutions Containing Elevated Pi Concentration. As introduced above, the concentration of Pi in human serum is in a dynamic state and can be elevated, even to a pathologically high level in some cases, e.g., the hyperphosphatemia of chronic kidney disease (CKD). Herein, we increased the Pi concentration in the reaction system from 2.00 to 5.00 mM to further investigate the effect of PPI on mineralization.

We find that at the Pi concentrations of 5.00 mM, the profiles of pH change curves are similar to those of normal Pi concentration (2.00 mM), and each one is divided into steps as

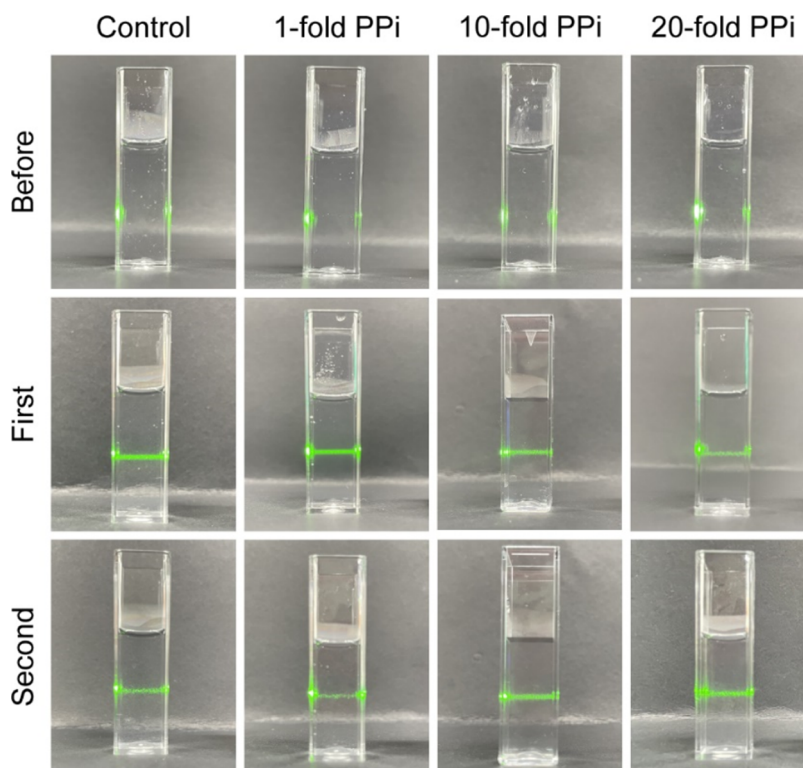


Figure 3. Tyndall effect tests of the titration solutions of 2.00 mM Pi with varied concentrations of PPI at different time points. Upper row: the solutions before the first pH inflection (labeled as Before); middle row: the solutions at the first pH inflection (labeled as First); and lower row: the solutions at the second pH inflection (labeled as Second). The exact sampling points are presented in Table S1.

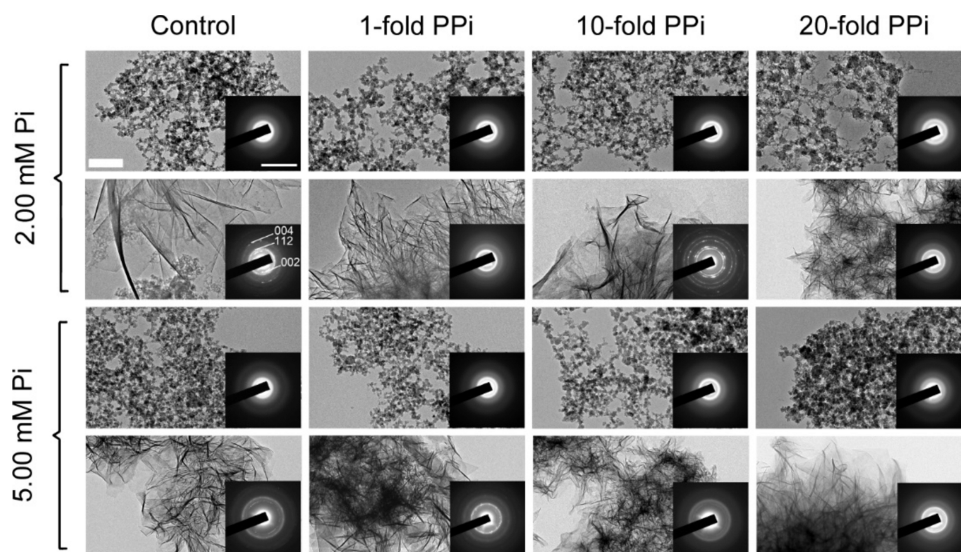


Figure 4. TEM images of the precipitates at different time points during titrations in Pi solutions. Precipitates were collected in solution of 2.00 mM Pi at the time points slightly after the first pH inflection (line 1) or slightly after the second pH inflection (line 2). Precipitates were collected in solution of 5.00 mM Pi at the time points slightly after the first pH inflection (line 3) or slightly after the second pH inflection (line 4). Scale bar of TEM micrographs: 200 nm. Scale bar of SAED patterns: 10 nm⁻¹. All SAED patterns correspond to the phase of hydroxyapatite, and the representative indexing of the diffractions is shown in the leftmost one of line 2. The exact sampling points are presented in Tables S1 and S2.

well (Figure 2A). However, the occurrence points of nucleation and crystallization are earlier (Figure 2B,C). In the control (absence of PPI), 1.19 ± 0.06 mM Ca²⁺ is needed to reach the first pH inflection and 1.97 ± 0.12 mM Ca²⁺ is required to reach the second, which are much lower than those in the 2.00 mM Pi solutions. Moreover, upon adding PPI in each Pi solution, the required Ca²⁺ concentration for

nucleation or crystallization is much lower than that (with the same PPI concentrations) in a 2.00 mM Pi solution as well.

Furthermore, we find that the addition of 1-fold PPI (1.7 μM) does not significantly inhibit the nucleation either. Indeed, 1.30 ± 0.12 mM Ca²⁺ is required to reach the nucleation point in the 1-fold PPI group, which is not significantly different from the control group ($p > 0.05$),

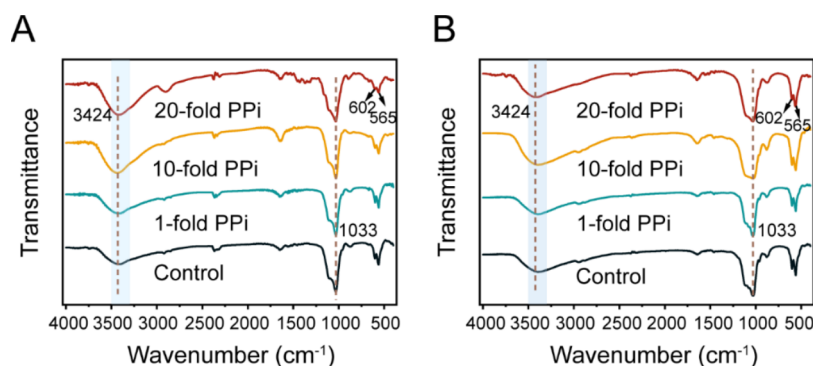


Figure 5. FTIR spectra of the precipitates collected after the second pH inflection in 2.00 (A) and 5.00 mM (B) Pi solutions. The exact sampling points are presented in Table S1 and S2.

similar to the effect in the 2.00 mM Pi solution. The addition of 10-fold PPI significantly inhibits the nucleation ($p < 0.01$), requiring 1.43 ± 0.03 mM to reach the nucleation, which is higher than that of the control (Figure 2A,B). Again, the 20-fold PPI does not see a distinct pH inflection at nucleation, although it is observed that the white turbidity forms at a time point very close to that of 10-fold PPI.

Like nucleation, PPI has a similar inhibitory effect on crystallization as well: 1-fold PPI (2.09 ± 0.15 mM Ca^{2+}) does not significantly inhibit crystallization compared to the solution without PPI (1.97 ± 0.12 mM Ca^{2+}) ($p > 0.05$), but 10-fold PPI (2.38 ± 0.10 mM Ca^{2+}) ($p < 0.01$) and 20-fold PPI (2.31 ± 0.12 mM Ca^{2+}) ($p < 0.05$) do (Figure 2C).

2.3. Characterization of the Species Formed during Titrations. The species in different steps of titrations were further characterized to find more information about the influences of PPI on mineral formation. Samples were collected in the solution before or after the pH inflections (see the specific time points for sampling in Tables S1 and S2) and then characterized in multiple ways.

First, Tyndall effects of the solutions (2.00 and 5.00 mM Pi; 0.050 M CaCl_2) used for titrations were detected with a laser beam to confirm that there was no light scattering from the original ions (Figure S1). Subsequently, the Tyndall effects of solutions during titration were tested. According to Figures 3 and S2, all solutions display no visible Tyndall effect before the first pH inflection but have a significant light path of scattering after that; this state is kept or even wider after the second pH inflection. These observations prove that the first pH inflection of all titration solutions above corresponds to mineral nucleation and initial precipitation.

Then, the morphology and phases of the species at each step were characterized (Figure 4). Both in the solution of 2.00 and 5.00 mM Pi, the transmission electron microscopy (TEM) images of the samples collected slightly after the first pH inflections of titrations (in the presence of 0, 1-fold, and 10-fold PPI) show the normal nanosphere-like (or their aggregation) morphology, whose amorphous phase is evident in the selected area electron diffraction (SAED) patterns without any diffraction signals. Additionally, with 20-fold PPI, additional amorphous nanowires are formed alongside the nanospheres, consistent with a previous study.⁵⁴ These observations indicate that the initial species after nucleation are amorphous calcium phosphate (ACP) in all of the titration procedures.

The morphology of the species after the second pH inflection of all titrations displays sheet-like (or their

aggregation) morphology whose crystalline states are corroborated by the SAED with significant diffraction rings or spots. Further indexing the diffractions indicates that they are hydroxyapatite, which thus proves the event of crystallization after the second pH inflection (Figure 4). The crystalline form of the species after the second pH inflection is also confirmed by Fourier transform infrared spectrometer (FTIR) measurements. On the FTIR spectra (Figure 5), the bands at 1033 cm^{-1} are attributed to the stretching vibration of P–O, while the split bands (not a single one) of P–O bending vibrations at 602 and 565 cm^{-1} are characteristic for crystalline calcium phosphates (Figure 5).⁵⁵

2.4. Concentration Changes of PPI during the Titrations. Following the performance of PPI on mineralization inhibition above, it raises the question how the concentration of PPI changes during titrations. Therefore, in the process of titration in 5.00 mM Pi, the supernatant (1 mL) extracted at different time points was assayed using a PPI kit to elucidate the changes (Figure 6). We find that in all solutions

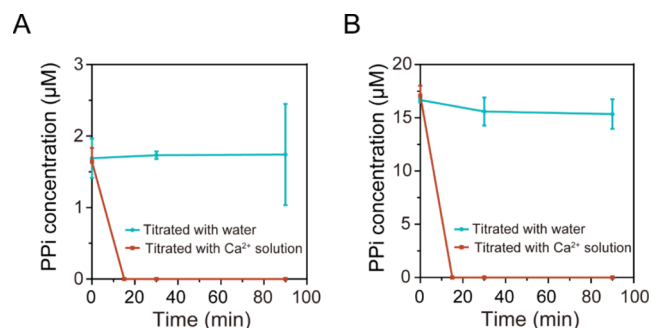


Figure 6. (A) PPI concentrations during titrating Ca^{2+} solution or water into the 5.00 mM Pi solution with initial 1.7 μM PPI. (B) PPI concentrations during titrating Ca^{2+} solution or water into the 5.00 mM Pi solution with initial 17 μM PPI.

containing 1-fold or 10-fold PPI, it is abruptly out of detection in the solution after nucleation and until the end of titration. In comparison, when titrating water (in the absence of Ca^{2+} , set as a control) into the solution, the concentration of PPI does not change significantly, thus indicating that it does not hydrolyze during the investigated time duration (Figure 6A,B). Therefore, we speculate that PPI may bind to or be occluded in the formed minerals during titration, leading to a sharp decrease in the concentration of PPI in the titration solution. Thus, it is reasonable that the weak inhibitory effect on the nucleation and crystallization by PPI of normal serum

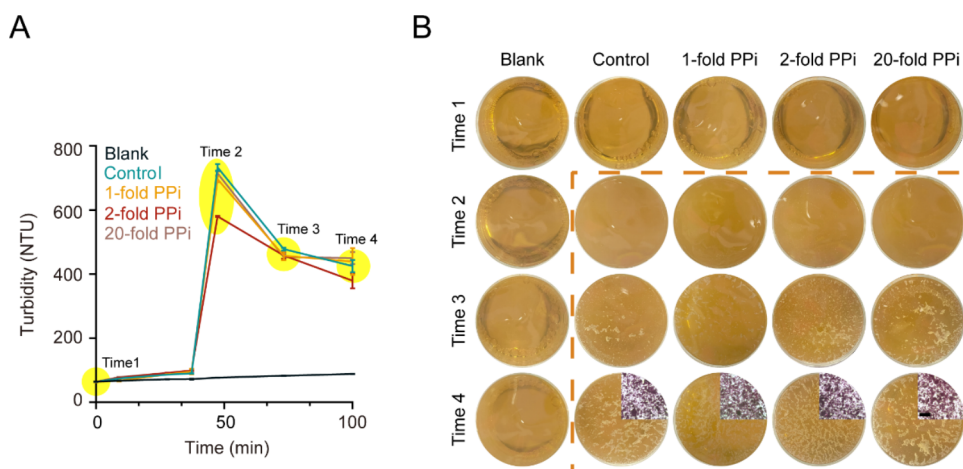


Figure 7. (A) Turbidity changes during titrating Ca^{2+} solution into the newborn calf serum containing different amounts of PPI. (B) Photographs of the white precipitates in the serum at the titration time points marked with yellow spots in (A). The samples in the orange dashed rectangles exhibit turbidity higher than 400 NTU. Inset: photographs of the Alizarin red-stained precipitates obtained at time 4. Scale bar: 400 μm . The formed minerals at time 2 are in the state of colloids; therefore, big particles were not observed in the photographs. Blank: the serum without PPI addition is titrated with pure water (in the absence of Ca^{2+}) into it. Control: the serum without PPI addition is titrated with Ca^{2+} solution into it.

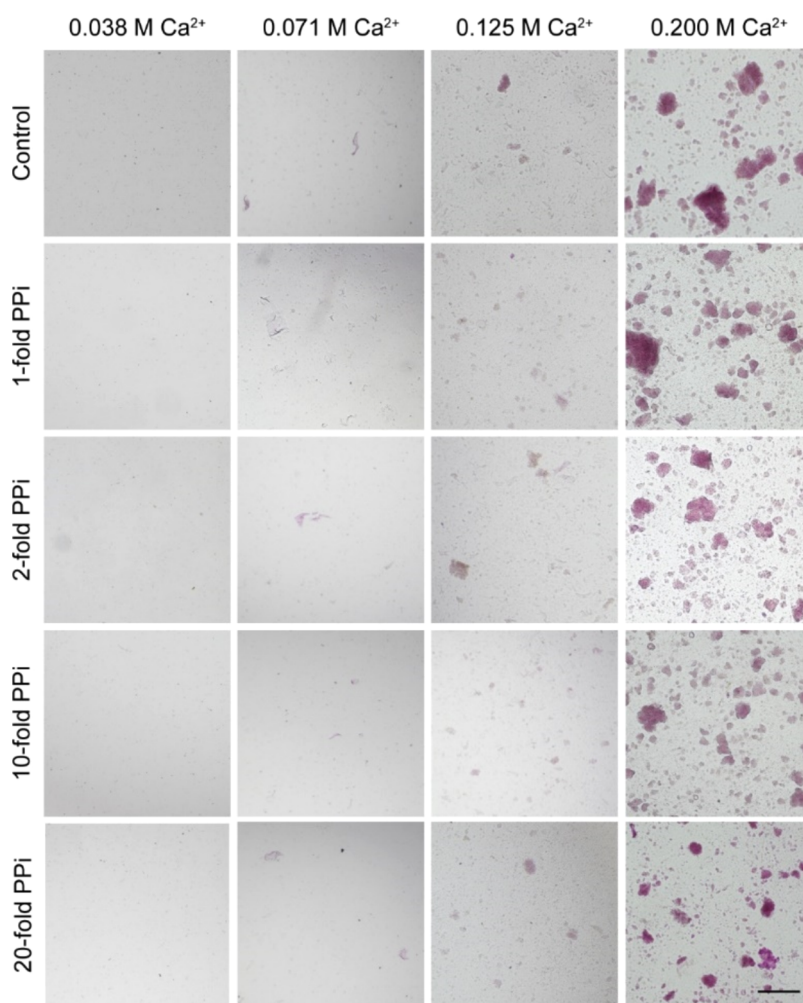


Figure 8. Photographs of the Alizarin red-stained precipitates obtained by adding different amounts of Ca^{2+} ions into newborn calf serum, which was incubated at 37 $^{\circ}\text{C}$ for 1 h. Scale bar: 400 μm . Control: the serum is free of PPI addition before the addition of Ca^{2+} ions.

concentrations may be attributed to the insufficient amount of such ions in the initially formed precipitates.

2.5. Ability of PPI to Inhibit Mineralization in Serum. The studies described above are performed in aqueous solutions of inorganic ions, but the composition of serum is

much more complex, containing a variety of small and big biomolecules. Hence, it is necessary to verify the influence of PPI on mineralization in real serum.

Like in aqueous solutions, mineralization in serum was studied upon titrating the Ca^{2+} solution in it (Figure 7A). We note that the pH change during titrating Ca^{2+} into serum (newborn calf serum) is smooth and has no significant inflection on the curves, leading to the failure of monitoring the mineralization process from the pH change. However, the turbidity during titration can be detected to reveal the formation of minerals. Therefore, we tracked the turbidity change in serum as an alternative of pH change. Briefly, PPI was added in the newborn calf serum to get the PPI-increased one; then, a solution of calcium chloride (2.00 M) was titrated into the newborn calf serum at a slow rate (1.00 mL/h) to induce precipitates of calcium phosphate, which were meanwhile monitored by measuring the turbidity of the serum at different time points. In the blank group where the serum is free of PPI addition and pure water (in the absence of Ca^{2+}) is titrated in it, the turbidity increases slightly (from 64.5 ± 0.55 NTU at the beginning to 88.1 ± 0.53 NTU at the end) and very few precipitates are observed (Figure 7B). However, when titrating Ca^{2+} solution into the serum (control), there is a burst turbidity increase after 47 min (732 ± 10.3 NTU), whereby a significant white precipitate is observed and its component of calcium phosphate is confirmed by alizarin red staining (selectively binding to the calcium salts, inset of Figure 7B), indicating that the increase of Ca^{2+} to a certain concentration can indeed generate mineralization in serum. However, introduction of PPI into serum beforehand, irrespective of the concentration of 1-fold or 20-fold, does not delay the burst turbidity increase (Figure 7A,B) during the titration of Ca^{2+} under the same conditions. This shows that PPI, in the studied concentration range, including the normal serum concentration, has no significant inhibitory effect on such mineral formation in serum.

Mineralization in serum was also studied upon incubation after direct addition of Ca^{2+} (Figure 8). Specifically, we introduced different amounts of PPI (1-fold, 2-fold, 10-fold, and 20-fold) into newborn calf serum, followed by direct addition (not slow titration) of the Ca^{2+} solution. After incubating the serum at 37 °C for 1 h, the formed minerals were collected by centrifugation and stained with Alizarin red for observation. The precipitates were compared between PPI-increased serum (experimental group) and the normal one (free of PPI addition, control). When the precipitates are observed with an optical microscope, no Alizarin red-stained calcium phosphate is found when 0.038 M CaCl_2 is added in both control and experimental groups, indicating that the very few precipitates in this case may not be calcium phosphate but proteins. However, when the added calcium ions reach 0.071 M or higher, obvious calcium phosphate solids, which can be stained by Alizarin red, are observed. We find that all of the observations find no significant difference in the investigated groups (with and without PPI addition, even at 20-fold concentration) regarding the required amount of added Ca^{2+} ions for precipitation. This further confirms the weak performance of serum PPI of normal concentration in resisting mineralization.

It should be noted that although 10-fold and 20-fold PPI displays inhibition against mineralization in the aqueous solution, such effects are not observed in serum. As introduced above, serum contains a variety of biomolecules and ions, so

some of them may be more critical than PPI in such performance depending on their types and concentrations. Thus, this finding reveals that PPI in serum may act as a mineralization inhibitor either at a much higher concentration, e.g., >20-fold (but would also bring the concerns of side effects) or via other pathways, e.g., serum serves as a transporter of PPI to deliver it to other tissues.

3. CONCLUSIONS

In summary, this study reveals that PPI with a normal serum concentration may not be able to inhibit mineralization in serum. This is demonstrated via a chemical titration process in an aqueous Pi solution of different concentrations and in serum. During the titrations, the normal serum concentration of PPI does not delay either nucleation or crystallization of calcium phosphate minerals, although the 10-fold or higher concentrations of PPI do. Furthermore, in the newborn calf serum, addition of neither 1-fold nor 20-fold PPI can significantly inhibit mineral formation compared to the normal serum. Thus, PPI in serum may function at a much higher concentration or via alternative mechanisms for inhibiting mineralization.

We note that (1) this study does not deny the importance of PPI in the inhibition of in vivo mineralization but suggests that it should be considered from other perspectives and (2) while these investigations mainly mimic the mineral formation in serum, they should be also meaningful for that in other tissues, such as cartilages and ligaments. For future work, further explorations from other perspectives in the real serums and in vivo models should be conducted to elucidate the specific roles of PPI in biomineralization.

4. EXPERIMENTAL SECTION

4.1. Materials and Apparatus. A pyrophosphate assay kit with enhanced selectivity (AAT Bioquest); disodium hydrogen phosphate (ACS reagent, $\geq 99.0\%$, Sigma); calcium chloride dihydrate (AR, 99%, Bioss antibodies); sodium pyrophosphate (PPI) (AR, 99%, Aladdin); hydrochloric acid (AR, 36.0–38.0%, Sinopharm Chemical Reagent); sodium hydroxide (AR, 99%, Aladdin); ethylene glycol (AR, 98%, RHAWN); potassium bromide anhydrous (AR, 99%, Aladdin); newborn calf serum (AusgeneX, Australia); and Alizarin red S solution (0.2%, Solarbio) were used.

A pH meter (PXSJ-216F, Leici, China); SpectraMaxiD5 (Molecular Devices); collective heat magnetic stirrer (DF-101S, VRERA, China); microporous filter (0.45 μM , Millipore); Fourier transform infrared spectrometer (FTIR) (Shimadzu Corporation, Tokyo, Japan); mini-pellet press (GS01150, UHUA TECHNOLOGY, China); Mikro-Spritzpumpen (LINZ-9B, Leien, China); transmission electron microscope (TEM, JEOLJEM-2100, Japan) equipped with selected area electron diffraction (SAED); and turbidimeter (LH-Z10A, LOHAND, China) were used.

4.2. Experimental Methods. **4.2.1. Study of Mineralization in Aqueous Solutions via Titration.** The experiments were conducted by titrating a 0.05 M CaCl_2 solution into the Na_2HPO_4 solutions with normal (2.00 mM, resembling the normal concentration in human serum) or higher (5.00 mM, resembling the abnormal concentration in human serum) concentrations. The turning points (denoted as inflections) between the change steps of pH curves were confirmed by differential processing.

Control: the pH of the Na_2HPO_4 solution was adjusted to 7.4 with HCl solution (1:1 diluted), and then, 0.05 M CaCl_2 solution was titrated into it with a highly accurate syringe pump at a rate of 5.00 mL/h, during which the pH change was monitored with a pH meter.

The inhibitory effects of PPI on mineralization: Additional $\text{Na}_2\text{P}_2\text{O}_7$ (source of PPI) at 1, 2, 10, and 20 times the PPI concentration in human serum (1.7, 3.4, 17, and 34 μM , denoted as 1-fold, 2-fold, 10-fold, and 20-fold, respectively) was added to the Na_2HPO_4 solutions with the same concentrations as the control; then, the pH was adjusted to 7.4. Afterward, titration was performed with the same procedure as for the control.

All solutions were prepared with deionized water and immediately filtered through a 0.45 μm -pore size microporous filter to remove any possible particle impurities. Glassware was thoroughly rinsed with deionized water before use, and containers were always covered during drying to exclude dust particles that might act as nucleation agents for mineral formation.

4.2.2. Test of PPI Concentration. The concentration of PPI in the reaction solution was determined by using the PPI assay kit. In this assay, the PPI concentration was determined by the complex formed by PPI and a PPI sensor molecule, which was measured at $E_x/E_m = 370:470$ nm (cutoff = 455 nm), and the value of the fluorescence intensity was positively associated with the concentration of PPI. A total of 50 μL of sample and 50 μL of PPI sensor working solution were added to each well of a 96-well plate, then mixed gently and incubated at room temperature for 30 min while being protected from light before the absorbance measurement.

4.2.3. TEM and SAED. Each sample (1 mL) was collected at a certain time point during the titration process and immediately mixed with 1 mL of ethylene glycol to quench the reaction (without causing additional precipitates of the salts). Samples were immediately centrifuged at 10,000 rpm for 1 min, and the supernatant was discarded, washed twice with ethylene glycol, and then washed twice with anhydrous ethanol. The samples were dispersed in alcohol and were characterized using TEM and SAED.

4.2.4. FTIR. Samples were collected in the same way as for TEM, then dried at 37 $^\circ\text{C}$, mixed with KBr powder and ground, pressed with a pellet press to make a disk, and measured on an FTIR spectrometer in the wavenumber range of 400–4500 cm^{-1} .

4.2.5. Tyndall Effect. In brief, 2 mL of the reaction solutions was taken at certain time points during the titration, then added to the cuvette, and illuminated with a laser pointer. Meanwhile, a photograph of lighter scattering was captured with a digital camera.

4.2.6. Turbidity Test. A turbidimeter was applied to record the turbidities of the solutions. The turbidimeter utilizes a beam of light (860 nm) that passes through a cuvette containing the sample to be tested with two sensors to measure the intensities of both scattered and transmitted lights. The intensity ratio of the scattered and transmitted lights is proportional to the turbidity in the sample over a range of concentrations. The measurement value is expressed in NTU (nephelometric turbidity units).

4.2.7. Study of Mineralization in Serum. Serum was thawed at 4 $^\circ\text{C}$, centrifuged, filtered with a microporous filter (Millipore, 0.45 μm) to remove protein precipitates, and then preheated in a 37 $^\circ\text{C}$ water bath for 10 min before further use.

Mineralization in serum was first studied by titrating a Ca^{2+} solution into it. Additional PPI (from $\text{Na}_2\text{P}_2\text{O}_7$) at different concentrations was added to the newborn calf serum prior to titration, while the one without adding PPI was set as the control. The titrations were conducted by dropping 2.00 M CaCl_2 solution into the newborn calf serum at a slow rate (1.00 mL/h) in the 37 $^\circ\text{C}$ water bath, and the turbidity and precipitates of serum were detected using a turbidimeter at different time points. The serum was centrifuged at 10,000 rpm for 2 min, and then, the precipitates were collected, washed twice with water, and stained with Alizarin red (0.2% Alizarin red S solution) to confirm the mineral component (calcium phosphate). Afterward, the stained precipitates were immersed in 1 mL of water and gently blown with a pipette to make them evenly dispersed in the aqueous medium, and the dispersion was added to a 96-well plate (200 μL /well) and immediately viewed under an optical microscope.

Mineralization in serum was further studied upon incubation after addition of Ca^{2+} solution. In the control group, aqueous CaCl_2 solution (0.050 M) of four different volumes was separately added to 15.0 mL of newborn calf serum, so that the resulting serum includes additional Ca^{2+} of 0.625, 1.25, 2.50, and 5.00 mmol, and then, the mixture was incubated in a constant-temperature incubator at 37 $^\circ\text{C}$. After 1 h, the serum was centrifuged at 10,000 rpm for 2 min; then, the precipitates were collected, washed twice with water, and stained with Alizarin red (0.2% Alizarin red S solution) to confirm the mineral component (calcium phosphate). Afterward, the stained precipitates were immersed in 1 mL of water and gently blown with a pipette to make them evenly dispersed in the aqueous medium; then, the dispersion was added to a 96-well plate (200 μL /well) and immediately viewed under an optical microscope. In the experimental group, PPI solutions were added to the serum (the resulting concentrations were 1.7, 3.4, 17, and 34 μM) before adding CaCl_2 , and other conditions were kept the same as those of the control.

4.2.8. Statistical Analysis. Experimental groups were represented by three or more parallel samples to provide a mean value and standard deviation. Statistical analysis was conducted using Origin 8.0 and Graph Pad Prism 6 softwares. Differences between groups were tested with one-way analysis of variance (ANOVA) at 95% confidence interval, followed by Tukey multiple comparisons and post hoc tests. Statistical significance was set at $P < 0.05$. *, **, ***, and **** represent $p < 0.05$, $p < 0.01$, $p < 0.001$, and $p < 0.0001$, respectively.

■ ASSOCIATED CONTENT

Supporting Information

The Supporting Information is available free of charge at <https://pubs.acs.org/doi/10.1021/acsomega.3c10427>.

Sampling points presented on the pH change curves and Tyndall effect tests on the investigated solutions (PDF)

■ AUTHOR INFORMATION

Corresponding Authors

Xi Chen – Department of Preventive Dentistry, Shanghai Ninth People's Hospital, Shanghai Jiao Tong University School of Medicine, Shanghai 200011, P. R. China; Email: chenx1853@sh9hospital.org.cn

Feng Chen – Suzhou First People's Hospital, School of Medicine, Anhui University of Science and Technology, Huainan 232000 Anhui, P. R. China; Center for

Orthopaedic Science and Translational Medicine, Department of Orthopedic, Spinal Pain Research Institute, Shanghai Tenth People's Hospital, School of Medicine, Tongji University, Shanghai 200072, P. R. China; orcid.org/0000-0002-1162-1684; Email: fchen@tongji.edu.cn

Bing-Qiang Lu – Center for Orthopaedic Science and Translational Medicine, Department of Orthopedic, Spinal Pain Research Institute, Shanghai Tenth People's Hospital, School of Medicine, Tongji University, Shanghai 200072, P. R. China; orcid.org/0000-0002-7027-0351; Email: bqlu@tongji.edu.cn

Authors

Yuxuan Cheng – Suzhou First People's Hospital, School of Medicine, Anhui University of Science and Technology, Huainan 232000 Anhui, P. R. China

Jing Ru – Suzhou First People's Hospital, School of Medicine, Anhui University of Science and Technology, Huainan 232000 Anhui, P. R. China

Chaobo Feng – Center for Orthopaedic Science and Translational Medicine, Department of Orthopedic, Spinal Pain Research Institute, Shanghai Tenth People's Hospital, School of Medicine, Tongji University, Shanghai 200072, P. R. China

Xiaohao Liu – Center for Orthopaedic Science and Translational Medicine, Department of Orthopedic, Spinal Pain Research Institute, Shanghai Tenth People's Hospital, School of Medicine, Tongji University, Shanghai 200072, P. R. China

Hua Zeng – Center for Orthopaedic Science and Translational Medicine, Department of Orthopedic, Spinal Pain Research Institute, Shanghai Tenth People's Hospital, School of Medicine, Tongji University, Shanghai 200072, P. R. China

Shuo Tan – Center for Orthopaedic Science and Translational Medicine, Department of Orthopedic, Spinal Pain Research Institute, Shanghai Tenth People's Hospital, School of Medicine, Tongji University, Shanghai 200072, P. R. China

Complete contact information is available at:

<https://pubs.acs.org/10.1021/acsomega.3c10427>

Notes

The authors declare no competing financial interest.

ACKNOWLEDGMENTS

This work was financially supported by the National Key R&D Program of China (2022YFE0123500), the National Natural Science Foundation of China (52272304, 31771081), the Science and Technology Commission of Shanghai Municipality (21ZR1449700, 22S31903300), the Science and Technology Bureau of Suzhou City (SZKJXM202318), and the Open Project of Shanghai Key Laboratory of Magnetic Resonance in East China Normal University (SKMR2023A02).

REFERENCES

- (1) Anderson, H. C. Matrix vesicles and calcification. *Curr. Rheumatol. Rep.* **2003**, *5*, 222–226.
- (2) Murshed, M. Mechanism of Bone Mineralization. *Cold Spring Harbor Perspect. Med.* **2018**, *8*, No. a031229.
- (3) Reznikov, N.; Bilton, M.; Lari, L.; Stevens, M. M.; Kröger, R. Fractal-like hierarchical organization of bone begins at the nanoscale. *Science* **2018**, *360*, No. eaao2189.
- (4) Zimmermann, E. A.; Ritchie, R. O. Bone as a Structural Material. *Adv. Healthcare Mater.* **2015**, *4*, 1287–1304.
- (5) Erdemir, D.; Lee, A. Y.; Myerson, A. S. Nucleation of Crystals from Solution: Classical and Two-Step Models. *Acc. Chem. Res.* **2009**, *42*, 621–629.
- (6) Gebauer, D.; Kellermeier, M.; Gale, J. D.; Bergström, L.; Cölfen, H. Pre-nucleation clusters as solute precursors in crystallisation. *Chem. Soc. Rev.* **2014**, *43*, 2348–2371.
- (7) Von Euw, S.; Ajili, W.; Chan-Chang, T.-H.-C.; Delices, A.; Laurent, G.; Babonneau, F.; Nassif, N.; Azaïs, T. Amorphous surface layer versus transient amorphous precursor phase in bone – A case study investigated by solid-state NMR spectroscopy. *Acta Biomater.* **2017**, *59*, 351–360.
- (8) Gelli, R.; Ridi, F.; Baglioni, P. The importance of being amorphous: calcium and magnesium phosphates in the human body. *Adv. Colloid Interface Sci.* **2019**, *269*, 219–235.
- (9) Lotsari, A.; Rajasekharan, A. K.; Halvarsson, M.; Andersson, M. Transformation of amorphous calcium phosphate to bone-like apatite. *Nat. Commun.* **2018**, *9*, No. 4170.
- (10) Ulian, G.; Moro, D.; Valdrè, G. Hydroxylapatite and Related Minerals in Bone and Dental Tissues: Structural, Spectroscopic and Mechanical Properties from a Computational Perspective. *Biomolecules* **2021**, *11*, No. 728.
- (11) Wang, B.; Zhang, Z.; Pan, H. Bone Apatite Nanocrystal: Crystalline Structure, Chemical Composition, and Architecture. *Biomimetics* **2023**, *8*, No. 90.
- (12) Rey, C.; Combes, C.; Drouet, C.; Glimcher, M. J. Bone mineral: update on chemical composition and structure. *Osteoporosis Int.* **2009**, *20*, 1013–1021.
- (13) Kaleta, B. The role of osteopontin in kidney diseases. *Inflammation Res.* **2019**, *68*, 93–102.
- (14) Kapustin, A. N.; Chatrou, M. L. L.; Drozdov, I.; Zheng, Y.; Davidson, S. M.; Soong, D.; Furmanik, M.; Sanchis, P.; Rosales, R. T. M. D.; Alvarez-Hernandez, D.; Shroff, R.; Yin, X.; Muller, K.; Skepper, J. N.; Mayr, M.; Reutelingsperger, C. P.; Chester, A.; Bertazzo, S.; Schurgers, L. J.; Shanahan, C. M. Vascular Smooth Muscle Cell Calcification Is Mediated by Regulated Exosome Secretion. *Circ. Res.* **2015**, *116*, 1312–1323.
- (15) Voelkl, J.; Luong, T. T.; Tuffaha, R.; Musculus, K.; Auer, T.; Lian, X.; Daniel, C.; Zickler, D.; Boehme, B.; Sacherer, M.; Metzler, B.; Kuhl, D.; Gollasch, M.; Amann, K.; Müller, D. N.; Pieske, B.; Lang, F.; Alesutan, I. SGK1 induces vascular smooth muscle cell calcification through NF- κ B signaling. *J. Clin. Invest.* **2018**, *128*, 3024–3040.
- (16) Liu, Z.; Dong, N.; Hui, H.; Wang, Y.; Liu, F.; Xu, L.; Liu, M.; Rao, Z.; Yuan, Z.; Shang, Y.; Feng, J.; Cai, Z.; Li, F. Endothelial cell-derived tetrahydrobiopterin prevents aortic valve calcification. *Eur. Heart J.* **2022**, *43*, 1652–1664.
- (17) Huang, J.; Pu, Y.; Zhang, H.; Xie, L.; He, L.; Zhang, C.-L.; Cheng, C. K.; Huo, Y.; Wan, S.; Chen, S.; Huang, Y.; Lau, C. W.; Wang, L.; Xia, Y.; Huang, Y.; Luo, J.-Y. KLF2 Mediates the Suppressive Effect of Laminar Flow on Vascular Calcification by Inhibiting Endothelial BMP/SMAD1/5 Signaling. *Circ. Res.* **2021**, *129*, e87–e100.
- (18) Darrieutort-Laffite, C.; Blanchard, F.; Le Goff, B. Calcific tendonitis of the rotator cuff: From formation to resorption. *Joint Bone Spine* **2018**, *85*, 687–692.
- (19) Durham, A. L.; Speer, M. Y.; Scatena, M.; Giachelli, C. M.; Shanahan, C. M. Role of smooth muscle cells in vascular calcification: implications in atherosclerosis and arterial stiffness. *Cardiovasc. Res.* **2018**, *114*, 590–600.
- (20) Lee, S. J.; Lee, I.-K.; Jeon, J.-H. Vascular Calcification—New Insights into Its Mechanism. *Int. J. Mol. Sci.* **2020**, *21*, No. 2685.
- (21) Luo, H.; Li, Q.; Cao, Y.; Uitto, J. Therapeutics Development for Pseudoxanthoma Elasticum and Related Ectopic Mineralization Disorders: Update 2020. *J. Clin. Med.* **2021**, *10*, No. 114.
- (22) Baba, Y.; Broderick, D. F.; Uitti, R. J.; Hutton, M. L.; Wszolek, Z. K. Hereditary Brain Calcification Syndrome. *Mayo. Clin. Proc.* **2005**, *80*, 641–651.
- (23) Michigami, T.; Ozono, K. Roles of Phosphate in Skeleton. *Front. Endocrinol.* **2019**, *10*, No. 180.

- (24) Manghat, P.; Sodi, R.; Swaminathan, R. Phosphate homeostasis and disorders. *Ann. Clin. Biochem.* **2014**, *51*, 631–656.
- (25) Leung, J.; Crook, M. Disorders of phosphate metabolism. *J. Clin. Pathol.* **2019**, *72*, 741–747.
- (26) Kratz, A.; Lewandrowski, K. B. Case records of the Massachusetts General Hospital. Weekly clinicopathological exercises. Normal reference laboratory values. *N. Engl. J. Med.* **1998**, *339*, 1063–1072.
- (27) Kratz, A.; Lewandrowski, K. B. Normal Reference Laboratory Values. *N. Engl. J. Med.* **1998**, *339*, 1063–1072.
- (28) Moe, S. M. Calcium Homeostasis in Health and in Kidney Disease. *Compr. Physiol.* **2011**, *6*, 1781–1800.
- (29) Liu, H.; Huang, L.-H.; Sun, X.-Y.; Ouyang, J.-M. High-phosphorus environment promotes calcification of A7R5 cells induced by hydroxyapatite nanoparticles. *Mater. Sci. Eng., C* **2020**, *107*, No. 110228.
- (30) Sage, A. P.; Lu, J.; Tintut, Y.; Demer, L. L. Hyperphosphatemia-induced nanocrystals upregulate the expression of bone morphogenetic protein-2 and osteopontin genes in mouse smooth muscle cells in vitro. *Kidney Int.* **2011**, *79*, 414–422.
- (31) Smith, E. R.; Hewitson, T. D.; Jahnen-Dechent, W. Calciprotein particles: mineral behaving badly? *Curr. Opin. Nephrol. Hypertens.* **2020**, *29*, 378–386.
- (32) Kutikhin, A. G.; Feenstra, L.; Kostyunin, A. E.; Yuzhalin, A. E.; Hillebrands, J.-L.; Krenning, G. Calciprotein Particles. *Arterioscler., Thromb., Vasc. Biol.* **2021**, *41*, 1607–1624.
- (33) Atzeni, F.; Sarzi-Puttini, P.; Bevilacqua, M. Calcium Deposition and Associated Chronic Diseases (Atherosclerosis, Diffuse Idiopathic Skeletal Hyperostosis, and Others). *Rheum. Dis. Clin. North Am.* **2006**, *32*, 413–426.
- (34) Nakamura, E. I.; Uezono, Y.; Narusawa, K. I.; Shibuya, I.; Oishi, Y.; Tanaka, M.; Yanagihara, N.; Nakamura, T.; Izumi, F. ATP activates DNA synthesis by acting on P2X receptors in human osteoblast-like MG-63 cells. *Am. J. Physiol.-Cell Physiol.* **2000**, *279*, C510–C519.
- (35) Schäfer, C.; Heiss, A.; Schwarz, A.; Westenfeld, R.; Ketteler, M.; Floege, J.; Müller-Esterl, W.; Schinke, T.; Jahnen-Dechent, W. The serum protein $\alpha 2$ -Heremans-Schmid glycoprotein/fetuin-A is a systemically acting inhibitor of ectopic calcification. *J. Clin. Invest.* **2003**, *112*, 357–366.
- (36) Theuvsen, E.; Smit, E.; Vermeer, C. The Role of Vitamin K in Soft-Tissue Calcification. *Adv. Nutr.* **2012**, *3*, 166–173.
- (37) Barrett, H.; O’Keeffe, M.; Kavanagh, E.; Walsh, M.; O’Connor, E. M. Is Matrix Gla Protein Associated with Vascular Calcification? A Systematic Review. *Nutrients* **2018**, *10*, No. 415.
- (38) Orriss, I. R.; Arnett, T. R.; Russell, R. G. Pyrophosphate: a key inhibitor of mineralisation. *Curr. Opin. Pharmacol.* **2016**, *28*, 57–68.
- (39) Bäck, M.; Aranyi, T.; Cancela, M. L.; Carracedo, M.; Conceição, N.; Leftheriotis, G.; Macrae, V.; Martin, L.; Nitschke, Y.; Pasch, A.; Quaglino, D.; Rutsch, F.; Shanahan, C.; Sorribas, V.; Szeri, F.; Valdivielso, P.; Vanakker, O.; Kempf, H. Endogenous Calcification Inhibitors in the Prevention of Vascular Calcification: A Consensus Statement From the COST Action EuroSoftCalcNet. *Front. Cardiovasc. Med.* **2019**, *5*, No. 196.
- (40) Lust, G.; Seegmiller, J. E. A rapid, enzymatic assay for measurement of inorganic pyrophosphate in biological samples. *Clin. Chim. Acta* **1976**, *66*, 241–249.
- (41) Ryan, L. M.; Kozin, F.; Mccarty, D. J. Quantification of human plasma inorganic pyrophosphate. *Arthritis Rheum.* **1979**, *22*, 886–891.
- (42) Szeri, F.; Niaziorimi, F.; Donnelly, S.; Fariha, N.; Tertyshnaia, M.; Patel, D.; Lundkvist, S.; van de Wetering, K. The Mineralization Regulator ANKH Mediates Cellular Efflux of ATP, Not Pyrophosphate. *J. Bone Miner. Res.* **2020**, *37*, 1024–1031.
- (43) Jansen, R. S.; Küçükosmanoğlu, A.; de Haas, M.; Saphu, S.; Otero, J. A.; Hegman, I. E. M.; Bergen, A. A. B.; Gorgels, T. G. M. F.; Borst, P.; van de Wetering, K. ABCC6 prevents ectopic mineralization seen in pseudoxanthoma elasticum by inducing cellular nucleotide release. *Proc. Natl. Acad. Sci. U.S.A.* **2013**, *110*, 20206–20211.
- (44) Jansen, R. S.; Duijst, S.; Mahakena, S.; Sommer, D.; Szeri, F.; Váradi, A.; Plomp, A.; Bergen, A. A.; Elferink, R. P. J. O.; Borst, P.; Wetering, K. v. d. ABCC6-Mediated ATP Secretion by the Liver Is the Main Source of the Mineralization Inhibitor Inorganic Pyrophosphate in the Systemic Circulation—Brief Report. *Arterioscler., Thromb., Vasc. Biol.* **2014**, *34*, 1985–1989.
- (45) Ralph, D.; Levine, M.; Millán, J. L.; Uitto, J.; Li, Q. Weighing the Evidence for the Roles of Plasma Versus Local Pyrophosphate in Ectopic Calcification Disorders. *J. Bone Miner. Res.* **2020**, *38*, 457–463.
- (46) Ralph, D.; van de Wetering, K.; Uitto, J.; Li, Q. Inorganic Pyrophosphate Deficiency Syndromes and Potential Treatments for Pathologic Tissue Calcification. *Am. J. Pathol.* **2022**, *192*, 762–770.
- (47) Bergen, A. A. B.; Plomp, A. S.; Schuurman, E. J.; Terry, S.; Breuning, M.; Dauwerse, H.; Swart, J.; Kool, M.; van Soest, S.; Baas, F.; ten Brink, J. B.; de Jong, P. T. V. M. Mutations in ABCC6 cause pseudoxanthoma elasticum. *Nat. Genet.* **2000**, *25*, 228–231.
- (48) Habraken, W. J. E. M. The Integration of Ion Potentiometric Measurements with Chemical, Structural, and Morphological Analysis to Follow Mineralization Reactions in Solution. In *Methods in Enzymology*; Elsevier, 2013; Chapter 2, Vol. 532, pp 25–44.
- (49) Kellermeier, M.; Cölfen, H.; Gebauer, D. Investigating the Early Stages of Mineral Precipitation by Potentiometric Titration and Analytical Ultracentrifugation. In *Methods in Enzymology*; Elsevier, 2013; Chapter 3, Vol. 532, pp 45–69.
- (50) Schodder, P. I.; Gindele, M. B.; Ott, A.; Rückel, M.; Ettl, R.; Boyko, V.; Kellermeier, M. Probing the effects of polymers on the early stages of calcium carbonate formation by stoichiometric co-titration. *Phys. Chem. Chem. Phys.* **2022**, *24*, 9978–9989.
- (51) Sant, B. R.; Prasad, T. P. Determination of metallic iron, iron(II) oxide, and iron(III) oxide in a mixture. *Talanta* **1968**, *15*, 1483–1486.
- (52) Ruiz-Agudo, E.; Ruiz-Agudo, C.; Di Lorenzo, F.; Alvarez-Lloret, P.; Ibañez-Velasco, A.; Rodríguez-Navarro, C. Citrate Stabilizes Hydroxylapatite Precursors: Implications for Bone Mineralization. *ACS Biomater. Sci. Eng.* **2021**, *7*, 2346–2357.
- (53) Mekmene, O.; Rouillon, T.; Quillard, S.; Pilet, P.; Bouler, J.-M.; Pezennec, S.; Gaucheron, F. Effects of citrate and NaCl on size, morphology, crystallinity and microstructure of calcium phosphates obtained from aqueous solutions at acidic or near-neutral pH. *J. Dairy Res.* **2012**, *79*, 238–248.
- (54) Feng, C.; Lu, B. Q.; Fan, Y.; et al. Amorphous 1-D nanowires of calcium phosphate/pyrophosphate: A demonstration of oriented self-growth of amorphous minerals. *J. Colloid Interface Sci.* **2024**, *657*, 960–970.
- (55) Dorozhkin, S. V. Amorphous calcium (ortho)phosphates. *Acta Biomater.* **2010**, *6*, 4457–4475.